ACS OMEGA

Open Access

http://pubs.acs.org/journal/acsodf

Article

Boosting the Electrochemical Oxygen Evolution with Nickel Oxide Nanoparticle-Modified Glassy Carbon Electrodes in Alkaline Solutions

Alwaleed M. Alharthi, Omar A. Hazazi, Badreah A. Al Jahdaly, Mohammed A. Kassem,* and Mohamed I. Awad

Cite This: *ACS Omega* 2024, 9, 34927−34937

Read Online

ACCESS | Metrics & More | Article Recommendations

ABSTRACT: The present work investigates the electrocatalysis of oxygen evolution (OE) on a glassy carbon electrode modified with nickel oxide nanoparticles (NPs) (nano-Ni) in an alkaline solution. The nano-Ni is electrodeposited from an acidic sulfate electrolyte containing various additives, such as glucose, glycerol, and dimethyl glyoxime. The NPs are characterized morphologically and electrochemically using scanning electron microscopy and cyclic voltammetry. The elemental composition and electronic state of the modified electrodes were analyzed using X-ray photoelectron spectroscopy. A considerable enhancement in electrocatalytic activity, depending on the additives used, is observed. The study also explores the effect of nickel oxide loading to optimize the process. The highest cathodic shift in the onset potential of the oxygen evolution reaction is achieved with nickel oxide deposited in the presence of ethylene glycol.

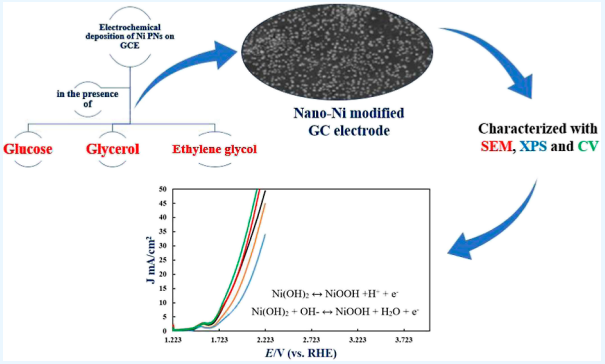

1. INTRODUCTION

Water splitting is crucial for alternative energy sources, including fuel cells. Its efficiency is influenced by the kinetics and thermodynamics of the hydrogen evolution reaction (HER) and the oxygen evolution (OE) reaction (OER). The OER, requiring an applied voltage exceeding 1.23 V vs RHE, is a rate-limiting step due to its complex mechanism and associated free energy.[1,2] The increased overvoltage results from the intricate OER mechanism on the anode surface under practical conditions.[3] Therefore, developing a suitable anode for OE must consider both thermodynamic and kinetic limitations.

Developing electrocatalysts for water oxidation is challenging due to the complexities of the OER. The goal in OER electrocatalysis research is to create efficient, cost-effective catalysts to replace expensive platinum-group oxides like RuO_2 and IrO_2. Transition metals such as Fe, Mn, and Ni are promising candidates due to their abundance and low cost.[4−9] To achieve specific nickel deposits, the composition of deposition solutions is controlled by adding certain additives. These additives help reduce roughness, control particle size, and achieve the desired microstructure in electrolytic nickel deposition, making the method suitable for particular applications.[10−13] In electrolytic nickel deposition, additives are also employed for the same reasons mentioned earlier, aiming to achieve a specific microstructure of the deposited nickel that is suitable for particular applications.[14−22]

This study investigates nickel deposition from a solution containing nickel ions and hydroxyl compounds, focusing on its application in OE. To modify the surface characteristics, structure, and morphology of nickel deposits, small amounts of organic additives are introduced to the plating baths.[23−26] These additives enhance the development of certain crystallite facets and may be incorporated into the deposits. While the role of additives in nickel deposition has been extensively studied, their impact on OE has not been thoroughly explored.[27−31] This research examines the effects of specific nonionic additives containing hydroxyl compounds on nickel deposition and their subsequent influence on OE, which for the first time to be reported for OE, addressing a gap in understanding their impact on critical fuel cell reactions, i.e., OE.[32−39] Unlike previous reports that address sophisticated methods, our work is simple and easy to be controlled. The

Received: May 17, 2024
Revised: July 26, 2024
Accepted: July 30, 2024
Published: August 3, 2024

present modification reveal significant improvements in the electrocatalytic activity and stability of NiO, thereby offering new insights into optimizing OER catalysts beyond conventional methods.

2. EXPERIMENTAL SECTION

2.1. Chemicals and Solutions. All chemicals utilized in this study were of analytical grade; reagent-grade sulfuric acid (H_2SO_4, 98%, density 1.84 g/mL), methanol (CH_3OH, 99.9%), nickel(II) sulfate hexahydrate ($NiSO_4{\cdot}6H_2O$, 99.9%), glucose, ethylene glycol (EG), and glycerol were procured from Sigma-Aldrich. Sodium hydroxide (NaOH, 99.8%) was obtained from BDH. All chemicals were used as received without further purification. Solutions were prepared using bidistilled water and, when necessary, were bubbled with nitrogen.

2.2. Instrumentation and Measurements. All electrochemical measurements were conducted using a Reference 600 potentiostat/galvanostat/ZRA. Voltammetric measurements were performed in a conventional three-electrode cell with a volume of approximately 20 mL. A platinum spiral wire served as the counter electrode, and an Ag/AgCl (KCl sat.) electrode was used as the reference electrode. The working electrode was a 3 mm glassy carbon (GC) disc (SigradurR-G, Sigri Electrographite GMBH, Germany) embedded in Teflon. All measurements were carried out at room temperature. The electrochemical behavior of the fabricated nickel nanoparticles (NPs) was analyzed using cyclic voltammetry, chronoamperometry, and Tafel analysis. Surface morphology was examined with a JEOL JSM 5410 scanning electron microscope (SEM), and X-ray photoelectron spectroscopy (XPS) measurements were performed using an ESCALABTM QXi X-ray Photoelectron Spectrometer Microprobe.

2.3. Pretreatment of Working Electrodes. The GC electrode was meticulously polished with sandpaper, starting with Grit 1500 and progressing to Grit 3000, until its surface appeared visually smooth. It was then rinsed with deionized water. Subsequently, the electrode was polished further using alumina powder with a particle size of 0.06 μm. Finally, the electrode underwent ultrasonic cleaning in pure deionized water for 15 min to remove any physically adsorbed species.

2.4. Preparation of the Modified Electrode. Before each experiment, a pretreatment step or a series of steps is performed to ensure the reproducibility of the surface introduced into the electrochemical cell. These steps may vary from basic mechanical polishing to scanning across a predefined potential range or exposure to a solvent or chemical species to "activate" the electrode. Following the cleaning of the GC electrode, as mentioned earlier, it is modified with nano-NiO_x as follows: nickel is electrodeposited from a solution containing 0.02 M $NiSO_4{\cdot}6H_2O$ at pH 4.5 by applying a certain potential for various durations. This pH value is chosen to mitigate the influence of the parasitic HER.[40] This electrode is designated as (GC_{ox}/nano-Ni). The nickel is prepared in the presence of different concentration of various hydroxyl compounds.

3. RESULTS AND DISCUSSION

3.1. Characterization of the Modified GC/NiO_x Electrode. Figure 1 shows SEM images of the GC/NiO_x samples fabricated under different conditions: (A) in the absence of additives, and in the presence of 50 mM of (B) glucose, (C) glycerol, and (D) EG. The choice to coat nickel NPs on GCE is well-founded. GCE was chosen as the substrate due to its stability and conductivity, which support uniform nickel NPs deposition. Its excellent electrical conductivity and chemical inertness minimize interference with electrochemical measurements. This makes GCE ideal for studying and optimizing the electrocatalytic properties of Ni NPs. These images depict the morphology and particle size distribution of the nickel NPs on the GC surface. The particle density of the nickel NPs is high when deposition is carried out in the presence of additives, indicating uniform deposition. The particle size is smallest in the presence of EG, with an average size of approximately 55 nm, while the additive-free sample has a spherical form with an average size of 100 nm.

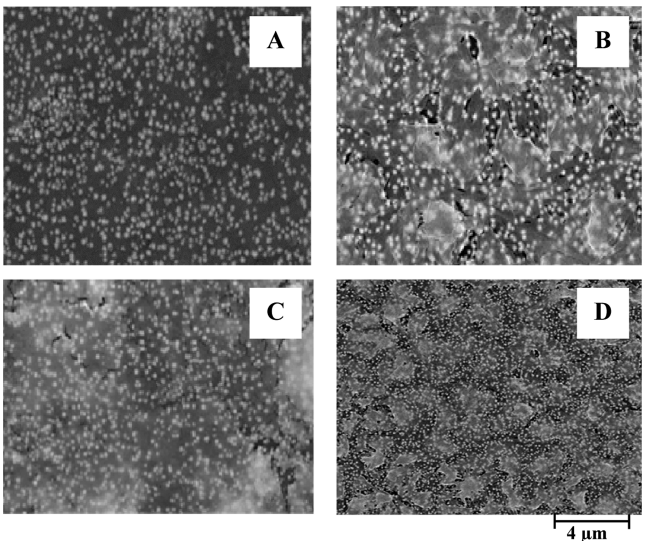

Figure 1. SEM images of the GC/NiO_x fabricated in (A) the absence, presence of 50 mM (B) glucose, (C) glycerol and (D) EG as additives.

Nickel deposition was performed using the chronoamperometric method, and the current−time relations (i−t) for the electrodeposition of nickel on GC electrodes are shown in Figure 2. Panel (a) represents deposition in the absence of glucose (GC/Ni), while panel (b) shows deposition in the presence of 50 mM glucose (GC/Ni-Glu), both at a constant potential of −0.8 V for 10 s. The two curves exhibit similar general features. The current rapidly increases to a peak before slightly decreasing, characteristic of metal nucleation and growth on the electrode surface. Initially, the electric double layer's charge causes a decrease in cathodic current. As nickel ions diffuse to the cathode and gain electrons, the cathodic current rises to a peak. Then, as the diffusion layer thickens, the cathodic current decreases.[41−44] The charge consumed in both cases was 16.3 and 17.2 mC, respectively. Assuming 100% Coulombic efficiency, the corresponding loading of nickel was estimated to be 63 and 67 μg cm^{-2} for GC/Ni and GC/Ni-Glu, respectively. The slightly higher deposition at GC/Ni-Glu indicates a higher reaction rate at that electrode. In the presence of EG, the charge consumed was 20.8 mC, corresponding to a loading of nickel of 20.4 μg cm^{-2}. For glycerol, the charge consumed was 11.4 mC, corresponding to a loading of nickel of 44.1 μg cm^{-2}.

Figure 3 shows cyclic voltammograms (CVs) for GC/Ni and GC/Ni-Glu in a 0.5 M NaOH solution. For both anodic and cathodic peaks, the peak current for the redox couple

https://doi.org/10.1021/acsomega.4c04700
ACS Omega 2024, 9, 34927−34937

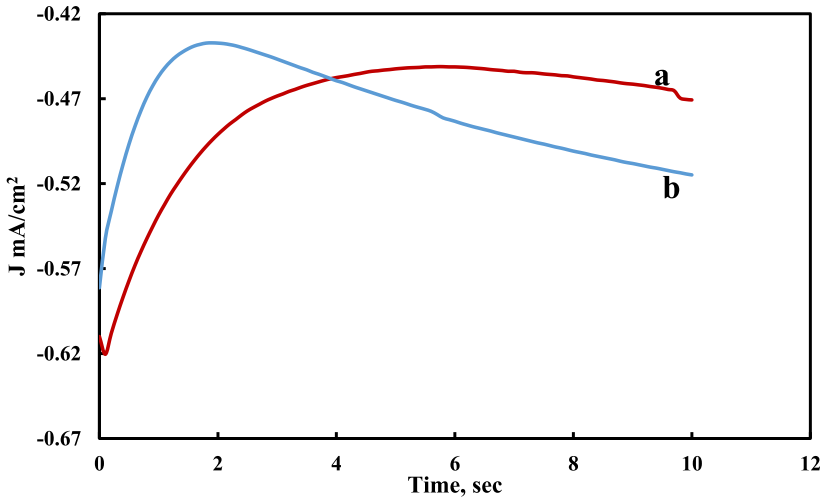

Figure 2. *i*−*t* curves obtained during nickel deposition at −0.8 V for 10 s. Glucose concentration: (a) 0.0 mM and (b) 50 mM.

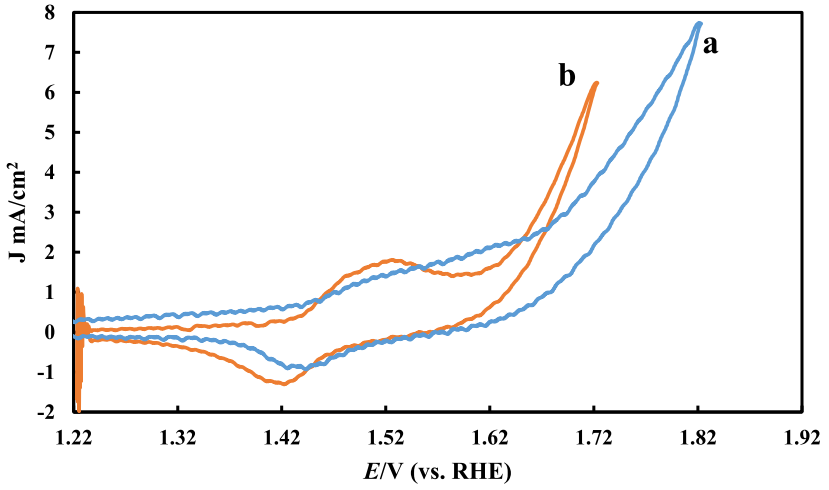

Figure 3. Cyclic voltammetry (CV) of nickel deposition in 0.5 M NaOH on a GC electrode: (a) without glucose and (b) with 50 mM glucose, at a scan rate of 100 mV/s.

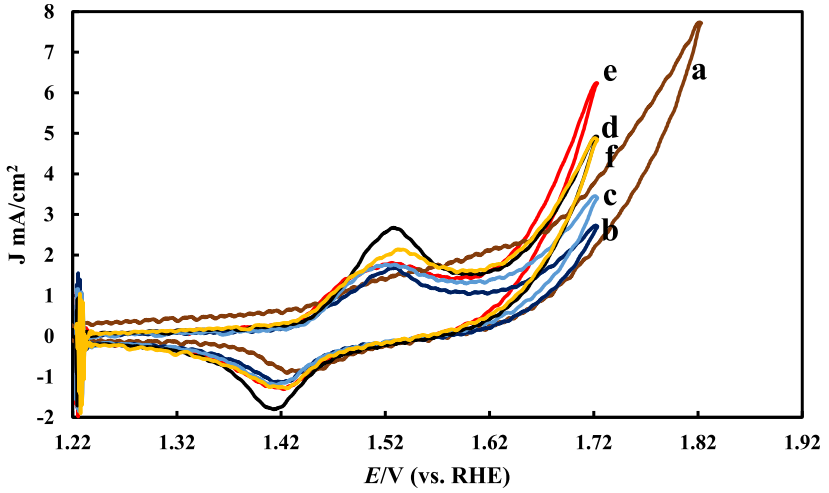

Figure 4. CVs for the nickel redox couple in 0.5 M NaOH using a nickel NP-modified GC electrode: (a) without glucose, (b) after oxidation, (c) with 10 mM glucose, (d) with 20 mM glucose, (e) with 30 mM glucose, and (f) with 50 mM glucose. All measurements were performed at a scan rate of 100 mV/s.

$(Ni(OH)_2 \leftrightarrow NiOOH)$ follows the order: GC/Ni < GC/Ni-Glu. This increase in peak current is attributed to the larger surface area of the NiO_x NPs, consistent with SEM findings that show smaller nickel particles deposited in the presence of

https://doi.org/10.1021/acsomega.4c04700
ACS Omega 2024, 9, 34927−34937

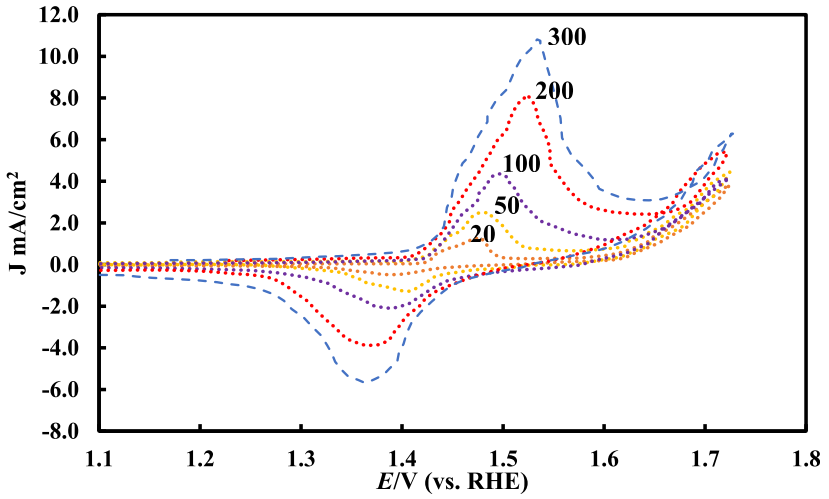

Figure 5. Effect of scan rate on the CV of GC/Ni-Glu, where nickel was deposited in the presence of 15 mM glucose, in 0.5 M NaOH. The scan rates are indicated in mV.

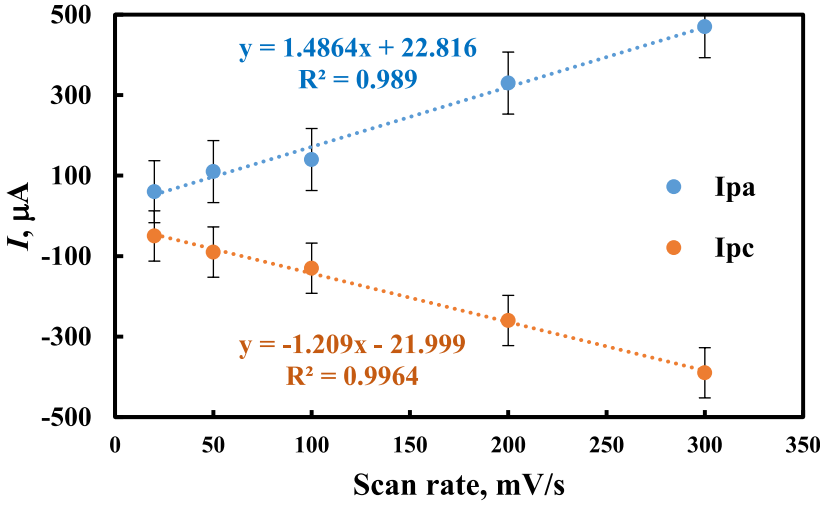

Figure 6. Relationship between peak current and scan rate.

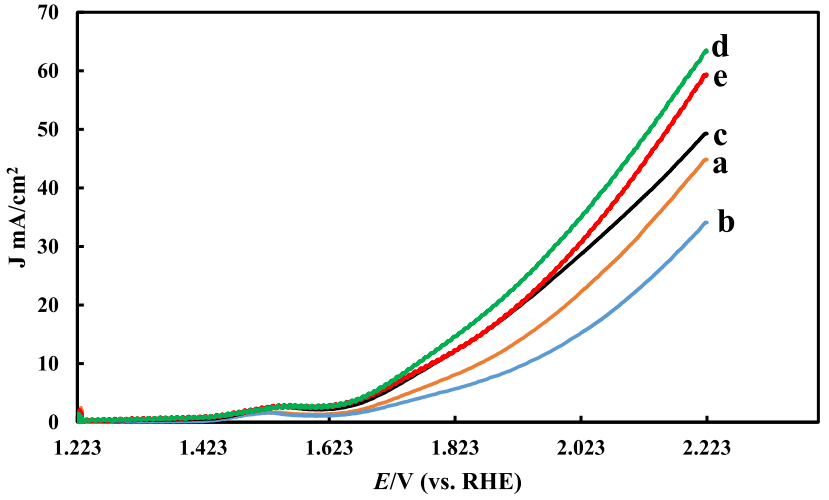

Figure 7. LSV for the OE reaction (OER) in 0.5 M NaOH using the GC electrode after nickel deposition: (a) without glucose, (b) after oxidation, and with glucose concentrations of (c) 20 mM, (d) 30 mM, and (e) 50 mM, all at a scan rate of 10 mV/s.

glucose compared to its absence. Additionally, the particle density is higher for the GC/Ni-Glu electrode. The surface concentration of active nickel sites (Γ) is estimated using the formula: $\Gamma = Q/(nF)$, where Q is the charge, n is the number of

https://doi.org/10.1021/acsomega.4c04700
ACS Omega 2024, 9, 34927−34937

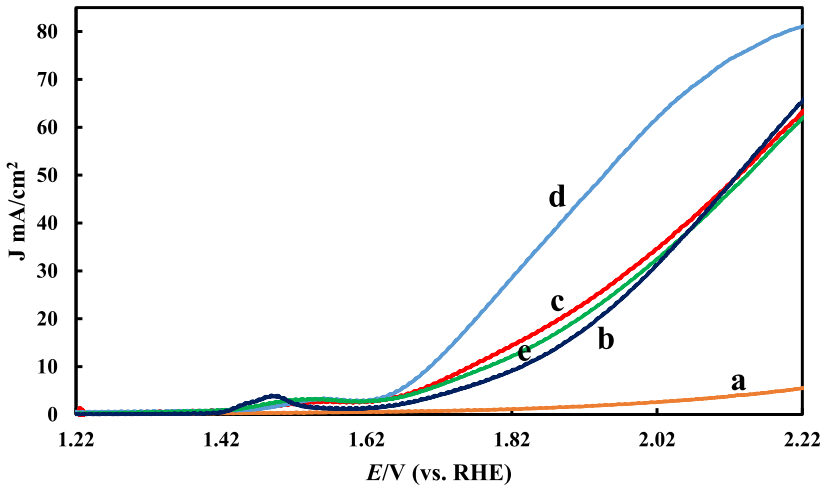

Figure 8. LSV for OE in 0.5 mM NaOH using (a) bare and (b−e) modified GC electrode. Ni deposition was conducted in the (b) absence and presence of 30 mM of (c) glucose, (d) EG and (e) glycerol at a scan rate 10 mV/s.

Scheme 1. Illustrated Mechanism for OER Using Nano-Ni Modified GCE in 0.5 M NaOH

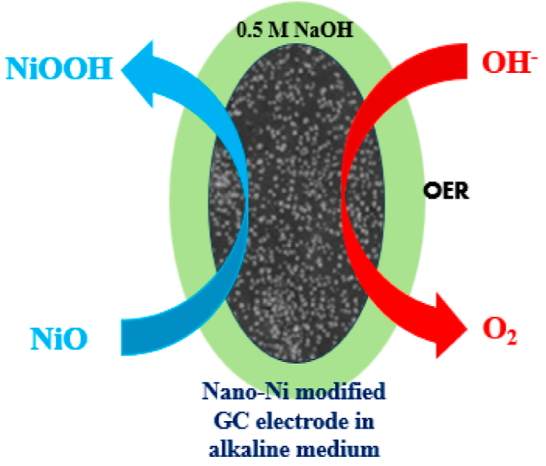

electrons transferred, and F is the Faraday constant.[45,46] The charge (Q) is derived from the area under the CV curve at a scan rate of 5 mV s^{-1}. The Γ values were found to be 12.0 and 12.6 nmol cm^{-2} for GC/Ni and GC/Ni-Glu, respectively, confirming the earlier conclusions.

The anodic and cathodic scans of nickel hydroxide electrodes produce various phases, including β-$Ni(OH)_2$, α-$Ni(OH)_2$, β-NiOOH, and γ-NiOOH.[47] The formation of γ-NiOOH is associated with the swelling of the nickel film, which can cause microcracks and eventual disintegration.[48] Therefore, β-NiOOH is considered a superior electroactive material for high electrochemical performance in alkaline solutions.[49] The conversion of Ni(II) to Ni(III) can proceed via two mechanisms: one involving proton diffusion, which typically forms β-NiOOH (eq 1), and the other involving solvent-mediated hydroxyl ion diffusion, leading to the formation of γ-NiOOH (eq 2).[50,51]

$$Ni(OH)_2 \leftrightarrow NiOOH + H + + e^- \quad (1)$$

$$Ni(OH)_2 + OH - \leftrightarrow NiOOH + H_2O + e^- \quad (2)$$

The charge (Q) calculated for nickel deposition from the nickel bath, both with and without 50 mM glucose, was determined by subtracting the charge consumed during the HER. This was done by performing the same experiment

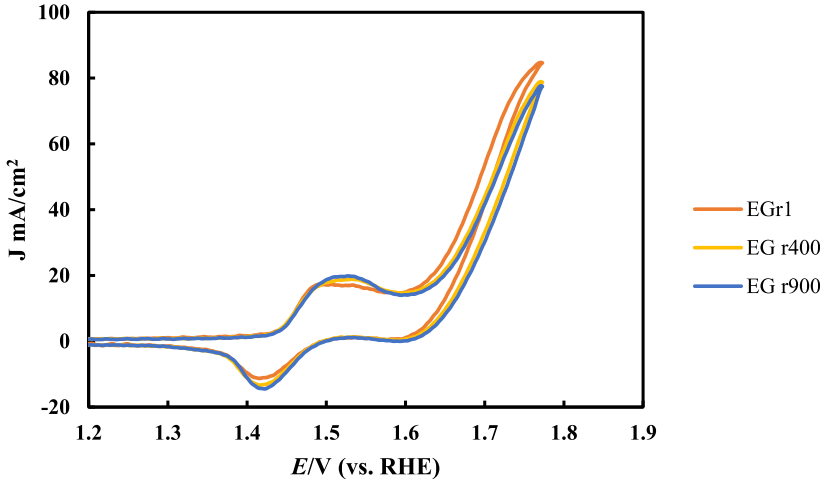

Figure 9. Continuous potential cycling of the GC/Ni-EG electrode (modified with nickel deposited from a 30 mM EG bath) at 1, 400, and 900 cycles.

https://doi.org/10.1021/acsomega.4c04700
ACS Omega 2024, 9, 34927−34937

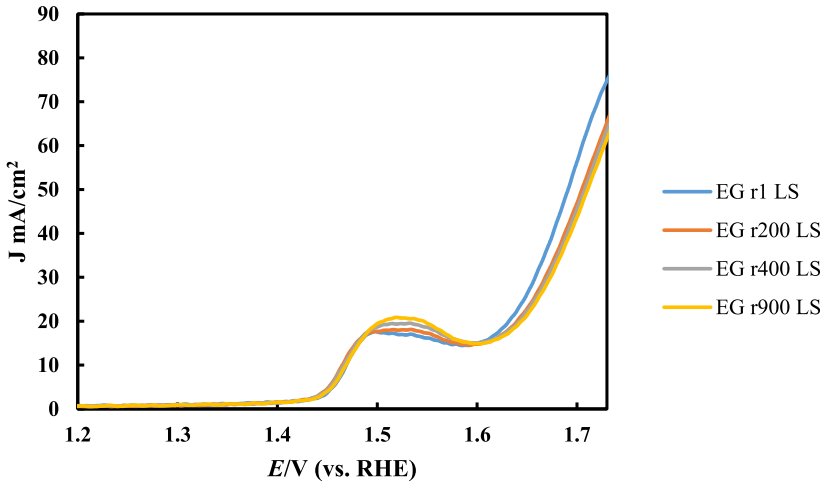

Figure 10. LSV results for the GC/Ni-EG electrode, with nickel deposition conducted in the presence of 30 mM EG, after continuous potential cycling for 1, 200, 400, and 900 cycles.

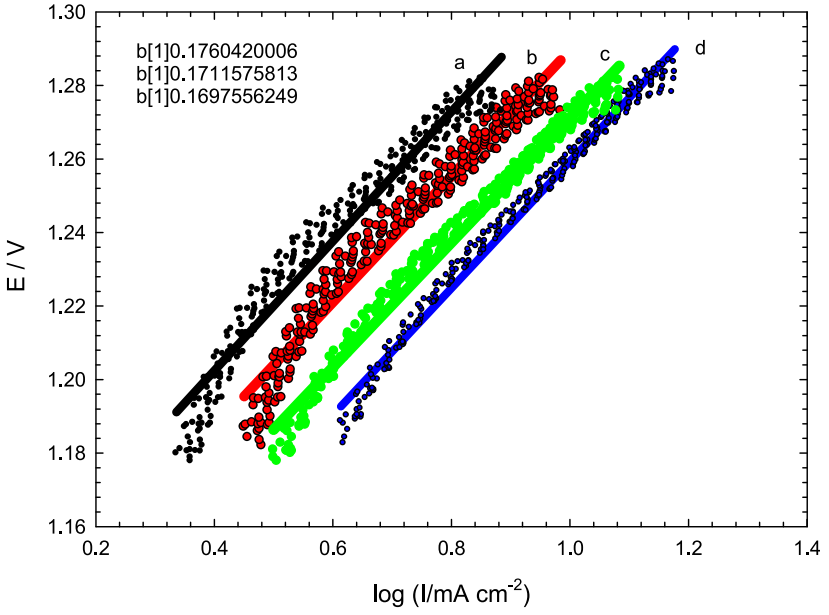

Figure 11. Tafel plots for the GC/Ni electrode in 0.5 M NaOH, where nickel was prepared (a) in the absence of additives and in the presence of (b) glycerol, (c) glucose, and (d) EG.

without the nickel ion source. The observed differences in peak current (i.e., the enhancement of the Ni(II)/Ni(III) redox couple) shown in Figure 3 are therefore attributed not to variations in NiO_x loading but to the distinct morphology and electrocatalytic activity of the electrode.

Figure 4 shows the CVs for GC/Ni-Glu in a 0.5 M NaOH solution with varying glucose concentrations. Nickel deposition was performed on both oxidized (curve *b*) and nonoxidized GC electrodes (curve *a*) for comparison. The GC electrode was oxidized by scanning the potential from −0.2 to 2 V over 5 cycles. The preoxidation of the GC electrode negatively affected the OE response. Therefore, nickel deposition in the presence of glucose was examined on nonoxidized GC electrodes (curves *c*−*e*). The results indicate that while increasing glucose concentration does not significantly affect the Ni^{2+}/Ni^{3+} redox couple, it markedly improves the rate of OE. This suggests that glucose has a notable impact on the phase of the deposited nickel oxide.

3.2. Effect of Scan Rate on the Nickel Modified Electrode. Figure 5 shows the effect of scan rate on the voltammetric behavior of GC/Ni, prepared in the presence of glucose, in a 0.5 M NaOH solution for electrochemical characterization. As the scan rate increases, both the cathodic and anodic peak currents rise, with the anodic peak potential shifting positively and the cathodic peak potential shifting negatively, demonstrating the quasi-reversible nature of the redox couple. Figure 6 presents the relationship between the peak currents (cathodic and anodic) and scan rate. The linear correlation observed indicates the adsorption nature of the Ni^{2+}/Ni^{3+} couple.[13,52−58]

3.3. Linear Scan Voltammetry Using the Nickel Modified Electrode. Figure 7 presents the catalytic performance of the OE reaction (OER) assessed using linear sweep voltammetry (LSV) at the GC/Ni electrode in 0.5 M NaOH. Nickel was deposited with various glucose concentrations, and the LSV plots are shown for: (a) no glucose, (b) after oxidation, (c) 20 mM glucose, (d) 30 mM glucose, and (e) 50

https://doi.org/10.1021/acsomega.4c04700
ACS Omega 2024, 9, 34927−34937

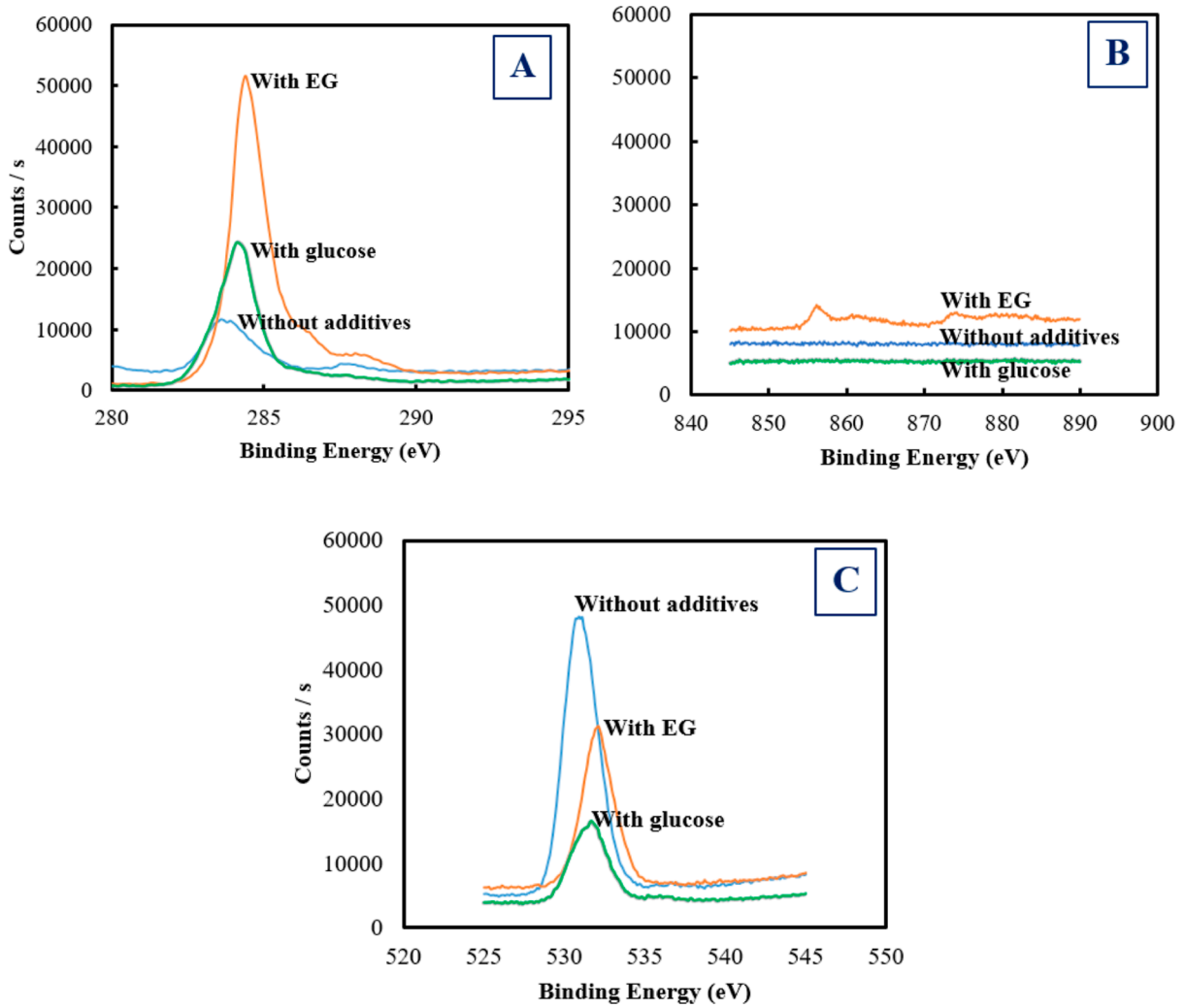

Figure 12. XPS spectra for the GC electrode modified with nickel, showing the effects of various additives. Panels: (A) C 1s, (B) Ni 2p, and (C) O 1s for samples prepared in the absence of additives, and in the presence of glucose, EG, and glycerol.

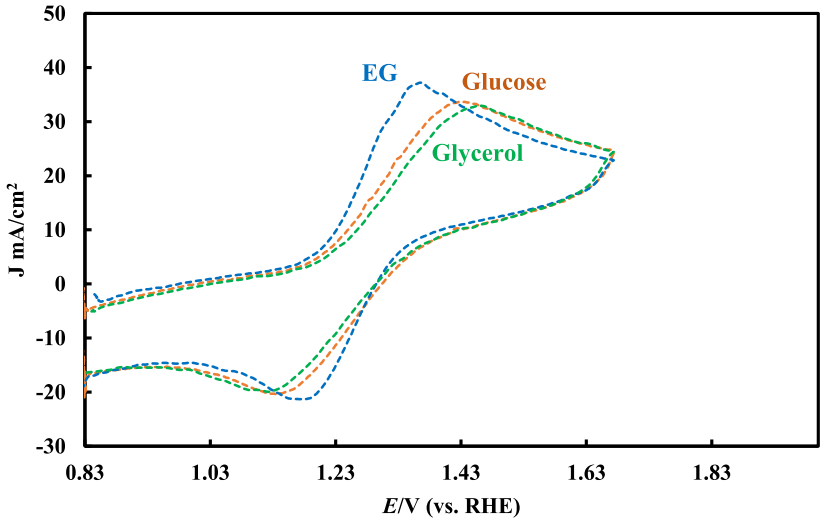

Figure 13. CVs of nickel NP-modified GC electrodes prepared with different additives in a 5 mM potassium ferrocyanide solution. Nickel deposition was performed in the presence of 30 mM glucose, glycerol, and EG, with a scan rate of 100 mV/s.

mM glucose, all at a scan rate of 10 mV/s. The onset potential of the OER shifts cathodically with increasing glucose concentration. Specifically, the overpotential required to sustain 10 mA cm^{-2} is 0.63 V for nickel deposited without glucose, 0.70 V after oxidation, and 0.56, 0.55, and 0.53 V for 20, 30, and 50 mM glucose, respectively. This demonstrates

https://doi.org/10.1021/acsomega.4c04700
ACS Omega 2024, 9, 34927−34937

the significant impact of glucose on the activity of the deposited nickel.

Figure 8 compares the effects of EG, glycerol, and glucose as additives on the OE performance at a nickel-modified electrode. LSV plots were obtained at the GC/Ni electrode in 0.5 M NaOH, with nickel prepared (b) in the absence of additives and in the presence of 30 mM of (c) glucose, (d) EG, and (e) glycerol, all at a scan rate of 10 mV/s. The onset potential of OER shifts cathodically to varying degrees depending on the hydroxyl compound used during nickel deposition. The largest shift is observed in the GC/Ni-EG curve (d), likely due to the smaller particle size as shown in the SEM images (Figure 1). A current density of 10 mA/cm^2 is commonly used as a benchmark for evaluating electrocatalytic materials for both hydrogen and OE reactions.[59,60] The overpotential needed to sustain 10 mA/cm^2 at the GC/Ni-EG electrode is 0.47 V, comparable to that of the IrO_2 electrode, which is a leading candidate for this application.[61] Recently, it has been reported that certain manganese cobalt and iron oxides demonstrate significantly better performance, even surpassing that of the benchmark IrO_2. This improvement is achieved by tuning modifier activity, which tailor the properties of the electrode for optimal mediation.[62−64]

3.4. Mechanism for the Understudy OER. The proposed mechanism for OER at the anode in alkaline conditions involves a series of reaction steps, which can be described as follows: the process begins with the anodic discharge of water molecules, leading to the formation of adsorbed hydroxyl radicals on the catalyst surface[65,66]

$$M + OH^- \rightarrow MOH + e^- \quad (3)$$

These adsorbed hydroxyl radicals then react to form metal oxide species

$$MOH + OH^- \rightarrow MO + H_2O + e^- \quad (4)$$

The metal oxide species further react with hydroxide ions to produce metal oxyhydroxide

$$MO + OH^- \rightarrow MOOH + e^- \quad (5)$$

Finally, the oxygen is formed through the formation and decomposition of MOOH intermediate.

$$MOOH + OH^- \rightarrow M + O_2 + H_2O + e^- \quad (6)$$

Nickel oxyhydroxide (NiOOH) is believed to play a crucial role in this mechanism. It participates in one or more of these steps through redox mediation. The NiOOH acts as an active site, facilitating the formation and decomposition of the MOOH intermediate, thereby aiding the OER process as illustrated in the following scheme (see Scheme 1).

3.5. Stability of the Modified Electrode. The stability of the modified electrode was assessed through continuous potential cycling, a widely recognized method for evaluating electrode stability.[67] Figure 9 presents CV results for GC/Ni-EG in NaOH, scanned over 900 cycles. The CV curves for cycles 1, 400, and 900 exhibit minimal variation, indicating consistent electrochemical stability throughout the cycling process. This demonstrates that the nickel NPs on GC maintain stability under these conditions, which is important for applications such as electrochemical sensors and energy storage devices. Additionally, Figure 10 shows the results of OE tests performed on the same electrode after continuous cycling. The data reveal that the performance of the electrode remained virtually unchanged after 900 cycles compared to the initial cycle, confirming that continuous cycling did not adversely affect the OE performance.

Figure 11 presents the Tafel plots derived from LSV curves to assess OER kinetics on the modified electrodes. The Tafel slopes were found to be 181 mV dec^{-1} for GC/Ni and 175 mV dec^{-1} for GC/Ni-Glu. The similar slopes suggest that the same mechanism is involved at both electrodes, although the GC/Ni-Glu electrode shows higher activity. Previous studies have indicated that additives in the deposition bath can significantly influence the morphology and phase of the deposited species, which in turn affects their performance as electrocatalysts for OE and other electrochemical reactions.[68]

To investigate the catalytic source, XPS was utilized, and the resulting data are presented in Figure 12. Elemental mapping was conducted on the spectra of nickel NPs across a binding energy range of 0 to 1200 eV, with graphs displaying the C 1s (panel A), Ni 2p (panel B), and O 1s (panel C) states. In panel A, a standard carbon peak (C 1s) at 284.80 eV was observed, with the mean peak for the graphitic carbon centered at 284 eV. The XPS spectra of the Ni 2p states for NPs fabricated in the absence and presence of additives are depicted in panel B. Notably, the Ni 2p core spectra were clearly discernible in the case of nickel deposited in the presence of EG, while in other samples, the Ni 2p peak was not as prominent, indicating more intensive deposition in the former case. It is noteworthy to mention that although the electrochemical behavior of the modified electrodes clearly indicates the deposition of nickel, as evidenced by the nickel couple shown in Figures 3 and 4, the peak corresponding to nickel in the XPS spectrum is not observed. This could be attributed to the low percentage loading of nickel NPs, consistent with literature.[69,70] This disparity could also indicate a difference in the chemical state, a hypothesis that could be verified by examining the oxygen peak (panel C). XPS has been shown to differentiate oxidation states based on binding energy peaks. The peaks obtained at approximately 854, 862, and 879 eV suggest Ni^{2+} states. The characteristic core level O 1s peaks for GC/Ni, GC/Ni-glu, and GC/Ni-EG are centered at 531, 532, and 533 eV, respectively, indicating different ratios of nickel oxidation states. The shift observed in GC/Ni-EG suggests the formation of an O−H group in the deposited NiO surface layer. Such shifts in binding energies could be the reason behind the differing activities of the deposited nickel.[71,72]

To further understand the catalytic properties of the modified electrodes, their voltammetric behavior in a ferrocyanide solution was examined and is presented in Figure 13. This figure shows CVs GCE modified with nickel NPs (Ni NPs), each prepared with different additives (glucose, glycerol, and EG) during electrodeposition. The CVs were recorded in a 5 mM potassium ferrocyanide solution, a well-known redox probe that exhibits a reversible one-electron process. The redox couple $[Fe(CN)_6]^{3-}/[Fe(CN)_6]^{4-}$ shows distinct oxidation and reduction peaks within the potential range of 1.0 to 1.5 V at a scan rate of 100 mV/s. The peak separation of 146 mV indicates quasi-reversible electrode behavior.[73] Among the electrodes tested, the one prepared in the presence of EG displayed the highest electrocatalytic activity, evidenced by the highest peak currents and the smallest peak separation. This enhanced activity suggests that EG improves the dispersion and reduces the particle size of Ni NPs, thereby increasing the surface area and number of active sites for redox reactions, as supported by SEM images (see Figure 1).

https://doi.org/10.1021/acsomega.4c04700
ACS Omega 2024, 9, 34927−34937

4. CONCLUSION

The electrochemical performance of nickel NP modified GC electrodes, prepared with various additives, provides key insights into their catalytic behavior for OE reaction. CV and LSV reveal that EG is the most effective additive, leading to the smallest particle size and highest electrocatalytic activity, evidenced by the lowest overpotential and highest current density. Glucose and glycerol also improve performance but to a lesser extent. Continuous potential cycling shows that the GC/Ni-EG electrode remains stable over 900 cycles, indicating its robustness for long-term use. Tafel analysis confirms similar catalytic mechanisms across different electrodes, with GC/Ni-Glu showing slightly enhanced activity. Redox behavior studies with potassium ferrocyanide reveal that GC/Ni-EG exhibits the highest electrocatalytic activity due to better dispersion and smaller particle size of Ni NPs. Overall, EG significantly enhances both the stability and catalytic activity of the electrodes, offering valuable insights for optimizing electrocatalysts in energy conversion and electrochemical sensing applications.

AUTHOR INFORMATION

Corresponding Author

Mohammed A. Kassem − *Chemistry Department, Faculty of Science, Umm Al-Qura University, Makkah 24382, Saudi Arabia; Chemistry Department, Faculty of Science, Benha University, Benha 13518, Egypt;* orcid.org/0000-0002-3775-3140; Phone: 00201554367071; Email: makassem@uqu.edu.sa, maa_kassem@hotmail.com

Authors

Alwaleed M. Alharthi − *Chemistry Department, Faculty of Science, Umm Al-Qura University, Makkah 24382, Saudi Arabia*

Omar A. Hazazi − *Chemistry Department, Faculty of Science, Umm Al-Qura University, Makkah 24382, Saudi Arabia*

Badreah A. Al Jahdaly − *Chemistry Department, Faculty of Science, Umm Al-Qura University, Makkah 24382, Saudi Arabia*

Mohamed I. Awad − *Chemistry Department, Faculty of Science, Umm Al-Qura University, Makkah 24382, Saudi Arabia; Chemistry Department, Faculty of Science, Cairo University, Cairo 12613, Egypt*

Complete contact information is available at: https://pubs.acs.org/10.1021/acsomega.4c04700

Notes

The authors declare no competing financial interest.

ACKNOWLEDGMENTS

The authors acknowledge the scientific and technical supports of Chemistry Department, Faculty of Science, Umm Al-Qura University, Makkah, Saudi Arabia for this research work.

REFERENCES

(1) Man, I. C.; Su, H. Y.; Calle-Vallejo, F.; Hansen, H. A.; Martínez, J. I.; Inoglu, N. G.; Kitchin, J.; Jaramillo, T. F.; Nørskov, J. K.; Rossmeisl, J. Universality in Oxygen Evolution Electrocatalysis on Oxide Surfaces. *ChemCatChem* **2011**, *3*, 1159−1165.

(2) Zhang, J.; Liu, J.; Xi, L.; Yu, Y.; Chen, N.; Sun, S.; Wang, W.; Lange, K. M.; Zhang, B. Single-Atom Au/NiFe Layered Double Hydroxide Electrocatalyst: Probing the Origin of Activity for Oxygen Evolution Reaction. *J. Am. Chem. Soc.* **2018**, *140*, 3876−3879.

(3) Strmcnik, D.; Lopes, P. P.; Genorio, B.; Stamenkovic, V. R.; Markovic, N. M. Design principles for hydrogen evolution reaction catalyst materials. *Nano Energy* **2016**, *29*, 29−36.

(4) Audichon, T.; Napporn, T. W.; Canaff, C.; Morais, C.; Comminges, C.; Kokoh, K. B. IrO_2 coated on RuO_2 as efficient and stable electroactive nanocatalysts for electrochemical water splitting. *J. Phys. Chem. C* **2016**, *120* (5), 2562−2573.

(5) Hong, W. T.; Risch, M.; Stoerzinger, K. A.; Grimaud, A.; Suntivich, J.; Shao-Horn, Y. Toward the rational design of non-precious transition metal oxides for oxygen electrocatalysis. *Energy Environ. Sci.* **2015**, *8* (5), 1404−1427.

(6) Qi, J.; Zhang, W.; Xiang, R.; Liu, K.; Wang, H. Y.; Chen, M.; Han, Y.; Cao, R. Porous nickel−iron oxide as a highly efficient electrocatalyst for oxygen evolution reaction. *Adv. Sci.* **2015**, *2* (10), 1500199.

(7) Li, F.; Shi, P.; Wu, J.; Qi, X.; Liu, Y.; Li, G. Trace Bimetallic Iron/Manganese Co-Doped N-Ketjenblack Carbon Electrocatalyst for Robust Oxygen Reduction Reaction. *J. Electrochem. Soc.* **2021**, *168*, 060502.

(8) Chen, Z.; Li, G.; Liu, Y.; Shi, P.; Li, F. Novel Co1-xS/C-3 supported on N-doped ketjen black as an efficient electrocatalyst for oxygen reduction reaction in alkaline media. *J. Taiwan Inst. Chem. Eng.* **2020**, *106*, 215−226.

(9) Li, F.; Chen, Z.; Shi, P.; Tan, P.; Li, G.; Liu, Y. Facile preparation of trace-iron doped manganese oxide/N-doped ketjenblack carbon composite for efficient ORR electrocatalyst. *J. Taiwan Inst. Chem. Eng.* **2019**, *100*, 230−238.

(10) Paunovic, M.; Schlesinger, M., *Fundamentals of Electrochemical Deposition*, 2nd ed.; John Wiley & Sons, 2006.

(11) Kim, S. K.; Bonevich, J. E.; Josell, D.; Moffat, T. P. Electrodeposition of Ni in submicrometer trenches. *J. Electrochem. Soc.* **2007**, *154* (9), D443.

(12) Kim, S.-K.; Josell, D.; Moffat, T. P. Electrodeposition of Cu in the PEI-PEG-Cl-SPS additive system: reduction of overfill bump formation during superfilling. *J. Electrochem. Soc.* **2006**, *153* (9), C616.

(13) Tantavichet, N.; Pritzker, M. D. Effect of plating mode, thiourea and chloride on the morphology of copper deposits produced in acidic sulphate solutions. *Electrochim. Acta* **2005**, *50* (9), 1849−1861.

(14) Walsh, F. C.; Low, C. T. J. A review of developments in the electrodeposition of tin. *Surf. Coat. Technol.* **2016**, *288*, 79−94.

(15) Abbott, A. P.; Ballantyne, A.; Harris, R. C.; Juma, J. A.; Ryder, K. S.; Forrest, G. A Comparative Study of Nickel Electrodeposition Using Deep Eutectic Solvents and Aqueous Solutions. *Electrochim. Acta* **2015**, *176*, 718−726.

(16) Wu, L. K.; Wang, W. K.; Cao, H. Z.; Hou, G. Y.; Tang, Y. P.; Zheng, G. Q. Electrodeposition of bright nickel from liquid ammonia solution containing chloride. *J. Electrochem. Soc.* **2016**, *163* (14), D829−D835.

(17) Gyawali, G.; Joshi, B.; Tripathi, K.; Lee, S. W. Effect of ultrasonic nanocrystal surface modification on properties of electrodeposited Ni and Ni-SiC composite coatings. *J. Mater. Eng. Perform.* **2017**, *26*, 4462−4469.

(18) Lanzutti, A.; Lekka, M.; De Leitenburg, C.; Fedrizzi, L. Effect of pulse current on wear behavior of Ni matrix micro-and nano-SiC composite coatings at room and elevated temperature. *Tribol. Int.* **2019**, *132*, 50−61.

(19) Cao, H.; Yang, D.; Zhu, S.; Dong, L.; Zheng, G. Preparation, characterization, and electrochemical studies of sulfur-bearing nickel in an ammoniacal electrolyte: the influence of thiourea. *J. Solid State Electrochem.* **2012**, *16*, 3115−3122.

(20) Burlyaev, D. V.; Tinaeva, A. E.; Tinaeva, K. E.; Kozaderov, O. A. Electrodeposition of zinc−nickel coatings from glycine-containing ammonium-chloride electrolyte. *Prot. Met. Phys. Chem.* **2020**, *56*, 552−559.

(21) Yue, M.; He, X.; Sun, S.; Sun, Y.; Hamdy, M. S.; Benaissa, M.; Salih, A. A.; Liu, J.; Sun, X. Co-doped Ni3S2 nanosheet array: A high-efficiency electrocatalyst for alkaline seawater oxidation. *Nano Res.* **2024**, *17*, 1050−1055.

(22) Liang, J.; Li, Z.; He, X.; Luo, Y.; Zheng, D.; Wang, Y.; Li, T.; Ying, B.; Sun, S.; Cai, Z.; Liu, Q.; Tang, B.; Sun, X. Electrocatalytic seawater splitting: Nice designs, advanced strategies, challenges and perspectives. *Mater. Today* **2023**, *69*, 193−235.
(23) De Almeida, M. R. H.; Barbano, E. P.; De Carvalho, M. F.; Tulio, P. C.; Carlos, I. A. Copper−zinc electrodeposition in alkaline-sorbitol medium: Electrochemical studies and structural, morphological and chemical composition characterization. *Appl. Surf. Sci.* **2015**, *333*, 13−22.
(24) Zhou, X.; Shen, Y. A novel method designed for electrodeposition of nanocrystalline Ni coating and its corrosion behaviors in Hank's solution. *Appl. Surf. Sci.* **2015**, *324*, 677−690.
(25) Ghaziof, S.; Gao, W. Electrodeposition of single gamma phased Zn−Ni alloy coatings from additive-free acidic bath. *Appl. Surf. Sci.* **2014**, *311*, 635−642.
(26) Awad, M.; Al-Hazemi, M. E.; Al-thagafi, Z. T. Glucose electrooxidation at nickel nanoparticles modified glassy carbon electrode: tolerance to poisoning. *Int. J. Electrochem. Sci.* **2022**, *17* (4), 220448.
(27) Hamilakis, S.; Balgis, D.; Milonakou-Koufoudaki, K.; Mitzithra, C.; Kollia, C.; Loizos, Z. Electrodeposition of CdSe photoabsorber thin films in the presence of selected organic additives. *Mater. Lett.* **2015**, *145*, 11−14.
(28) Bani Hashemi, A.; Kasiri, G.; La Mantia, F. The effect of polyethyleneimine as an electrolyte additive on zinc electrodeposition mechanism in aqueous zinc-ion batteries. *Electrochim. Acta* **2017**, *258*, 703−708.
(29) Zhu, Y. L.; Katayama, Y.; Miura, T. Effects of acetone and thiourea on electrodeposition of Ni from a hydrophobic ionic liquid. *Electrochim. Acta* **2012**, *85*, 622−627.
(30) Guo, J.; Guo, X.; Wang, S.; Zhang, Z.; Dong, J.; Peng, L.; Ding, W. Effects of glycine and current density on the mechanism of electrodeposition, composition and properties of Ni−Mn films prepared in ionic liquid. *Appl. Surf. Sci.* **2016**, *365*, 31−37.
(31) Wang, S.; Guo, X.; Yang, H.; Dai, J.; Zhu, R.; Gong, J.; Peng, L.; Ding, W. Electrodeposition mechanism and characterization of Ni−Cu alloy coatings from a eutectic-based ionic liquid. *Appl. Surf. Sci.* **2014**, *288*, 530−536.
(32) Ji, X.; Yan, C.; Duan, H.; Luo, C. Effect of phosphorous content on the microstructure and erosion−corrosion resistance of electrodeposited Ni-Co-Fe-P coatings. *Surf. Coat. Technol.* **2016**, *302*, 208−214.
(33) Zhu, Y. L.; Katayama, Y.; Miura, T. Effects of coumarin and saccharin on electrodeposition of Ni from a hydrophobic ionic liquid. *Electrochim. Acta* **2014**, *123*, 303−308.
(34) Zamani, M.; Amadeh, A.; Lari Baghal, S. Effect of Co content on electrodeposition mechanism and mechanical properties of electrodeposited Ni−Co alloy. *Met. Soc. China* **2016**, *26* (2), 484−491.
(35) Cârâc, G.; Ispas, A. Effect of nano-Al_2O_3 particles and of the Co concentration on the corrosion behavior of electrodeposited Ni−Co alloys. *J. Solid State Electrochem.* **2012**, *16* (11), 3457−3465.
(36) Yang, P.; Zhao, Y.; Su, C.; Yang, K.; Yan, B.; An, M. Electrodeposition of Cu−Li alloy from room temperature ionic liquid 1-butyl-3-methylimidazolium tetrafluoroborate. *Electrochim. Acta* **2013**, *88*, 203−207.
(37) Lopez, J. R.; Mendez, P. F.; Bueno, J. J. P.; Trejo, G.; Antano, R.; Torres-Gonzalez, J.; Stremsdoerfer, G.; Meas, Y. Samarium Additive Effect onto the Nickel Electrodeposition Process. *J. Electrochem. Soc.* **2017**, *164* (7), D524−D531.
(38) Bard, A. J.; Faulkner, L. R. *Electrochemical Methods: Fundamentals and Applications*, 2nd ed.; Wiley: New York, 1980.
(39) El-Refaei, S. M.; Awad, M. I.; El-Anadouli, B. E.; Saleh, M. M. Electrocatalytic glucose oxidation at binary catalyst of nickel and manganese oxides nanoparticles modified glassy carbon electrode: optimization of the loading level and order of deposition. *Electrochim. Acta* **2013**, *92*, 460−467.
(40) Schrebler Guzmán, R. S.; Vilche, J. R.; Arvia, A. J. Rate processes related to the hydrated nickel hydroxide electrode in alkaline solutions. *J. Electrochem. Soc.* **1978**, *125* (10), 1578−1587.
(41) Tan, C. y.; Liu, Y.; Zhao, X. s.; Zheng, Z. q. Nickel co-deposition with SiC particles at initial stage. *Trans. Nonferrous Met. Soc. China* **2008**, *18*, 1128−1133.
(42) Yu, Y.; Sun, L.; Ge, H.; Wei, G.; Jiang, L. Study on Electrochemistry and Nucleation Process of Nickel Electrodeposition. *Int. J. Electrochem. Sci.* **2017**, *12*, 485−495.
(43) Yao, Y.; Yang, C.; Sun, S.; Zhang, H.; Geng, M.; He, X.; Dong, K.; Luo, Y.; Zheng, D.; Zhuang, W.; Alfaifi, S.; Farouk, A.; Hamdy, M. S.; Tang, B.; Zhu, S.; Sun, X.; Hu, W. W. Boosting Alkaline Seawater Oxidation of CoFe-layered Double Hydroxide Nanosheet Array by Cr Doping. *Small* **2024**, *20*, No. e2307294.
(44) Zhang, H.; Han, H.; Yang, X.; Ma, H.; Song, Z.; Ji, X. Reversing Mg suppression effect on Co-site water oxidation of MgCo2O4 based on vanadium-atom electronic affinity synergy with Mg sites toward electronic redistribution. *Catal. Sci. Technol.* **2023**, *13*, 6951−6958.
(45) Giovanelli, D.; Lawrence, N. S.; Jiang, L.; Jones, T. G.; Compton, R. G. Electrochemical determination of sulphide at nickel electrodes in alkaline media: a new electrochemical sensor. *Sens. Actuators, B* **2003**, *88* (3), 320−328.
(46) Zhang, H.; He, X.; Dong, K.; Yao, Y.; Sun, S.; Zhang, M.; Yue, M.; Yang, C.; Zheng, D.; Liu, Q.; Luo, Y.; Ying, B.; Alfaifi, S.; Ji, X.; Tang, B.; Sun, X. Selenate promoted stability improvement of nickel selenide nanosheet array with an amorphous NiOOH layer for seawater oxidation. *Mater. Today Phys.* **2023**, *38*, 101249.
(47) Xing, W.; Li, F.; Yan, Z. F.; Lu, G. Q. Synthesis and electrochemical properties of mesoporous nickel oxide. *J. Power Sources* **2004**, *134* (2), 324−330.
(48) Dette, C.; Hurst, M. R.; Deng, J.; Nellist, M. R.; Boettcher, S. W. Structural Evolution of Metal (Oxy)hydroxide Nanosheets during the Oxygen Evolution Reaction. *ACS Appl. Mater. Interfaces* **2019**, *11*, 5590−5594.
(49) Wu, M. S.; Hsieh, H. H. Nickel oxide/hydroxide nanoplatelets synthesized by chemical precipitation for electrochemical capacitors. *Electrochim. Acta* **2008**, *53*, 3427−3435.
(50) El-Shafei, A. A. Electrocatalytic oxidation of methanol at a nickel hydroxide/glassy carbon modified electrode in alkaline medium. *J. Electroanal. Chem.* **1999**, *471* (2), 89−95.
(51) Abdel Rahim, M.; Abdel Hameed, R.; Khalil, M. W. Nickel as a catalyst for the electro-oxidation of methanol in alkaline medium. *J. Power Sources* **2004**, *134* (2), 160−169.
(52) Snook, G. A.; Duffy, N. W.; Pandolfo, A. G. Detection of oxygen evolution from nickel hydroxide electrodes using scanning electrochemical microscopy. *J. Electrochem. Soc.* **2008**, *155* (3), A262.
(53) Hu, Y.; Jin, J.; Wu, P.; Zhang, H.; Cai, C. Graphene−gold nanostructure composites fabricated by electrodeposition and their electrocatalytic activity toward the oxygen reduction and glucose oxidation. *Electrochim. Acta* **2010**, *56* (1), 491−500.
(54) Kwon, S. Y.; Kwen, H. D.; Choi, S. H. Fabrication of nonenzymatic glucose sensors based on multiwalled carbon nanotubes with bimetallic Pt-M (M= Ru and Sn) catalysts by radiolytic deposition. *J. Sens.* **2012**, *2012*, 1−8.
(55) Hui, S.; Zhang, J.; Chen, X.; Xu, H.; Ma, D.; Liu, Y.; Tao, B. Study of an amperometric glucose sensor based on Pd−Ni/SiNW electrode. *Sens. Actuators, B* **2011**, *155* (2), 592−597.
(56) He, C.; Han, X.; Kong, X.; Jiang, M.; Lei, D.; Lei, X. Fe-doped Co_3O_4@C nanoparticles derived from layered double hydroxide used as efficient electrocatalyst for oxygen evolution reaction. *J. Energy Chem.* **2019**, *32*, 63−70.
(57) Tie, L.; Liu, Y.; Shen, S.; Yu, C.; Sun, J.; Sun, J. Interface engineering of NiSe/Ni3S2 nanostructures as an efficient self-supported electrode for water oxidation in alkaline media. *Appl. Surf. Sci.* **2020**, *526*, 146745.
(58) Zhang, M.; Wang, T.; Cao, H.; Cui, S.; Du, P. Self-supported Ni_2P nanosheets on low-cost three-dimensional Fe foam as a novel electrocatalyst for efficient water oxidation. *J. Energy Chem.* **2020**, *42*, 71−76.

https://doi.org/10.1021/acsomega.4c04700
ACS Omega 2024, 9, 34927−34937

(59) Popczun, E. J.; McKone, J. R.; Read, C. G.; Biacchi, A. J.; Wiltrout, A. M.; Lewis, N. S.; Schaak, R. E. Nanostructured Nickel Phosphide as an Electrocatalyst for the Hydrogen Evolution Reaction. *J. Am. Chem. Soc.* **2013**, *135*, 9267−9270.
(60) Mcenaney, J. M.; Soucy, T. L.; Hodges, J. M.; Callejas, J. F.; Mondschein, J. S.; Schaak, R. E. Colloidally-synthesized cobalt molybdenum nanoparticles as active and stable electrocatalysts for the hydrogen evolution reaction under alkaline conditions. *J. Mater. Chem. A* **2016**, *4*, 3077−3081.
(61) McCrory, C. C. L.; Jung, S.; Peters, J. C.; Jaramillo, T. F. Benchmarking Heterogeneous Electrocatalysts for the Oxygen Evolution Reaction. *J. Am. Chem. Soc.* **2013**, *135*, 16977−16987.
(62) Sugawara, Y.; Kamata, K.; Ishikawa, A.; Tateyama, Y.; Yamaguchi, T. Efficient Oxygen Evolution Electrocatalysis on $CaFe_2O_4$ and Its Reaction Mechanism. *ACS Appl. Energy Mater.* **2021**, *4*, 3057−3066.
(63) Liu, C.; Qian, J.; Ye, Y.; Zhou, H.; Sun, C. J.; Sheehan, C.; Zhang, Z.; Wan, G.; Liu, Y. S.; Guo, J.; Li, S.; Shin, H.; Hwang, S.; Gunnoe, T. B.; Goddard, W. A.; Zhang, S. Oxygen evolution reaction over catalytic single-site Co in a well-defined brookite TiO_2 nanorod surface. *Nat. Catal.* **2021**, *4*, 36−45.
(64) Huang, Z. F.; Xi, S.; Song, J.; Dou, S.; Li, X.; Du, Y.; Diao, C.; Xu, Z. J.; Wang, X. Tuning of lattice oxygen reactivity and scaling relation to construct better oxygen evolution electrocatalyst. *Nat. Commun.* **2021**, *12*, 3992.
(65) Lyons, M. E. G.; Brandon, M. P. The oxygen evolution reaction on passive oxide covered transition metal electrodes in aqueous alkaline solution. Part 1-nickel. *Int. J. Electrochem. Sci.* **2008**, *3*, 1386−1424.
(66) Lyons, M. E. G.; Brandon, M. P. A comparative study of the oxygen evolution reaction on oxidised nickel, cobalt and iron electrodes in base. *J. Electroanal. Chem.* **2010**, *641*, 119−130.
(67) Shamsipur, M.; Najafi, M.; Hosseini, M. R. M. Highly improved electrooxidation of glucose at a nickel(II) oxide/multi-walled carbon nanotube modified glassy carbon electrode. *Bioelectrochemistry* **2010**, *77*, 120−124.
(68) Ju, X.; He, X.; Sun, Y.; Cai, Z.; Sun, S.; Yao, Y.; Li, Z.; Li, J.; Wang, Y.; Ren, Y.; Ying, B.; Luo, Y.; Zheng, D.; Liu, Q.; Xie, L.; Li, T.; Sun, X.; Tang, B. Fabrication of a hierarchical NiTe@NiFe-LDH core-shell array for high-efficiency alkaline seawater oxidation. *iScience* **2024**, *27*, 108736.
(69) Wang, W.; Liu, H.; Wu, T.; Zhang, P.; Ding, G.; Liang, S.; Jiang, T.; Han, B. Ru catalyst supported on bentonite for partial hydrogenation of benzene to cyclohexene. *J. Mol. Catal. A: Chem.* **2012**, *355*, 174−179.
(70) Mishra, D. K.; Dabbawala, A. A.; Hwang, J. S. Ruthenium nanoparticles supported on zeolite Y as an efficient catalyst for selective hydrogenation of xylose to xylitol. *J. Mol. Catal. A: Chem.* **2013**, *376*, 63−70.
(71) Soo Kim, D.; Chul Lee, H. Nickel vacancy behavior in the electrical conductance of nonstoichiometric nickel oxide film. *J. Appl. Phys.* **2012**, *112*, 034504.
(72) Kwon, U.; Kim, B. G.; Nguyen, D.; Park, J. H.; Ha, N. Y.; Kim, S. J.; Ko, S. H.; Lee, S.; Lee, D.; Park, H. J. Solution-Processible Crystalline NiO Nanoparticles for High-Performance Planar Perovskite Photovoltaic Cells. *Sci. Rep.* **2016**, *6*, 30759.
(73) Hassaninejad-Darzi, S. K.; Rahimnejad, M. Electrocatalytic oxidation of methanol by ZSM-5 nanozeolite-modified carbon paste electrode in alkaline medium. *J. Iran. Chem. Soc.* **2014**, *11*, 1047−1056.

https://doi.org/10.1021/acsomega.4c04700
ACS Omega 2024, 9, 34927−34937